

Proxy-Reliance Control in Conformal Recalibration of One-Sided Value-at-Risk

Tenghan Zhong, University of Southern California

tenghanz@usc.edu

Abstract

We introduce a proxy-reliance-controlled conformal recalibration framework for one-sided Value-at-Risk (VaR), and study a question that existing state-aware methods do not usually isolate: how strongly should the recalibration adjustment depend on an imperfect volatility proxy? We formalize this through a proxy-reliance parameter that continuously interpolates between an approximately constant-shift correction and a fully proxy-scaled correction. This makes proxy reliance a distinct and practically interpretable design choice in one-sided VaR recalibration.

We show theoretically that larger proxy reliance increases the responsiveness of the tail adjustment to proxy scale, but also increases stressed-state fragility when the proxy underreacts. Empirically, in rolling out-of-sample tests on a six-ETF panel with VIX-linked state variables, and with supporting evidence from SPY, we find that the empirical value of proxy-reliance control lies in improved stressed-state robustness rather than uniform overall dominance. In particular, when the baseline forecast remains exposed to proxy imperfection in stressed states, lower or intermediate proxy reliance can outperform fully proxy-scaled recalibration in stressed left-tail VaR control.

Keywords: Value-at-Risk; Conformal recalibration; Volatility proxy; Market stress; Tail risk

JEL Classification: C53, G17, G32

1 Introduction

Value-at-Risk (VaR) remains a standard tool for market risk measurement and capital assessment, even as the Basel market-risk framework has shifted internal-model regulation toward expected shortfall and more risk-sensitive capital standards [Basel Committee on Banking Supervision, 2019]. Yet reliable one-sided VaR control is especially difficult in the market conditions where protection matters most. Financial return distributions are nonstationary, tail behaviour changes across regimes, and forecast performance can deteriorate sharply in stressed episodes. As a result, methods that appear acceptable in pooled coverage may still fail where downside protection is most needed. A natural response is to incorporate volatility information into recalibration, but volatility signals are not ground truth. In practice they are informative yet imperfect, and their misspecification can become most consequential precisely in adverse states.

Recent conformal and state-aware recalibration methods address nonstationarity by allowing calibration to depend on time, state, or observation weights. This is an important advance, but it leaves open a distinct question that is central in financial risk management: when the state variable itself is an imperfect volatility proxy, how strongly should the recalibration correction depend on it? Existing approaches allow state information to enter the recalibration procedure, but they typically do not isolate the degree of dependence of the correction itself on proxy scale as a separate design object.

To address this, we develop a proxy-reliance-controlled conformal recalibration framework for one-sided left-tail VaR under imperfect volatility signals. Let $\widehat{q}_{\alpha,t}$ denote a baseline forecast of the lower α -quantile of next-period returns, and let v_t denote a positive volatility proxy. Our framework introduces a proxy-reliance parameter $\rho \in [0, 1]$ through the scaling rule v_t^ρ , so that $\rho = 0$ corresponds to an approximately constant correction, $\rho = 1$ corresponds to a fully proxy-scaled correction, and intermediate values provide a continuous compromise between state responsiveness and protection from proxy misspecification. In this way, the framework makes explicit a design margin that is usually left implicit in state-aware VaR methods: *proxy reliance*, namely, how strongly the recalibration correction inherits the scale of an imperfect volatility signal.

The paper makes three contributions. First, it identifies proxy reliance as a distinct design object in one-sided VaR recalibration and gives it a clear risk-management interpretation: larger values of ρ increase state responsiveness, but also increase exposure to proxy error. Second, it shows theoretically that ρ governs both the sensitivity of tail adjustment to proxy scale and stressed-state fragility under stress-specific proxy underreaction. Third, it evaluates this design margin empirically in a rolling out-of-sample study on a six-ETF panel with VIX-linked state information, with SPY retained as an illustrative benchmark. The evidence shows that proxy-reliance control is most valuable for stressed-state robustness rather than broad unconditional dominance. In particular, when residual stress-period undercoverage remains after the baseline forecast is formed and the volatility proxy underreacts in adverse states, lower or intermediate proxy reliance can outperform fully proxy-scaled recalibration in left-tail control. We also study a regime-aware extension with separate proxy-reliance levels across low-, medium-, and high-stress states, although its gains over simpler global stress-aware rules are limited and non-uniform.

The rest of the paper is organized as follows. Section 2 reviews the related literature. Section 3 describes the data and feature construction. Section 4 introduces the proxy-reliance-controlled recalibration framework and the regime-aware extension. Section 5 presents the empirical results, including stress-period analysis and proxy misspecification experiments. Section 6 discusses the implications for financial risk management and outlines directions for future research. Section 7 concludes.

2 Literature Review

2.1 VaR Forecasting, Dynamic Quantiles, and Backtesting

The VaR forecasting literature includes historical simulation, volatility-filtered methods, parametric conditional heteroskedastic models, and quantile-based predictive regressions. Standard approaches include historical simulation and volatility-updated or filtered historical simulation, as well as GARCH-type models that map time-varying volatility into conditional quantiles [Engle, 1982, Bollerslev, 1986, Hull and White, 1998, Barone-Adesi et al., 1999, Christof-

fersen, 2012]. Quantile regression provides a direct semiparametric alternative for modelling conditional tail behaviour from observed predictors [Koenker, 2005], while the CAViaR family models conditional quantile dynamics directly and remains an important benchmark for tail-risk forecasting [Engle and Manganelli, 2004]. More recent work extends the forecasting frontier toward high-frequency deep volatility models, adaptive machine-learning prediction of the VIX, option-surface-driven volatility forecasting, multivariate portfolio VaR–ES forecasting, and forward-looking physical tail-risk models [Moreno-Pino and Zohren, 2024, Bai and Cai, 2024, Michael et al., 2025, Storti and Wang, 2025, Zhang et al., 2026].

A central difficulty in this literature is that acceptable unconditional coverage does not guarantee reliable local performance. Financial applications also require attention to violation clustering and conditional adequacy, motivating standard backtesting tools such as the Kupiec unconditional coverage test, the Christoffersen conditional coverage test, and dynamic quantile diagnostics [Kupiec, 1995, Christoffersen, 1998, Engle and Manganelli, 2004]. Our paper is related to this literature, but shifts attention away from proposing another raw tail-forecasting engine and toward the design of a recalibration layer applied after the baseline forecast is formed. Once the focus moves from tail forecasting itself to post-hoc recalibration under nonstationarity, conformal methods become especially relevant because they provide a model-agnostic framework for uncertainty calibration under distributional instability.

2.2 Conformal Calibration under Dependence and Recent Financial Applications

Conformal prediction provides a distribution-free framework for uncertainty quantification and model-agnostic recalibration [Vovk et al., 2005, Angelopoulos and Bates, 2023]. While its classical guarantees rely on exchangeability, a growing literature studies conformal methods under dependence and nonstationarity through weighted, localized, adaptive, and sequential procedures [Chernozhukov et al., 2018, Gibbs and Candès, 2021, Bastani et al., 2022, Xu et al., 2024]. These developments are especially relevant in financial applications, where nonstationarity, heteroskedasticity, and regime shifts are intrinsic rather than exceptional.

Recent work has begun to apply adaptive conformal methods directly to financial risk fore-

casting. For example, adaptive conformal inference has been used to compute VaR across large panels of crypto-assets, emphasizing robustness under market instability. More recent work studies sequential one-sided VaR control through regime-weighted conformal risk control for nonstationary portfolio losses, while other recent studies develop temporal conformal prediction frameworks tailored to adaptive risk forecasting in financial time series [Fantazzini, 2024, Aich et al., 2025, Schmitt, 2026]. Related recent work also pushes conformal methods toward finance-specific decisions and risk functionals, including predictive portfolio selection and formalized real-time VaR estimation [Kato, 2024, Wang et al., 2026]. These contributions move conformal calibration in finance toward explicitly time-varying, state-aware, sequential, and decision-aware designs. Our paper is closest to this emerging literature, but addresses a different gap. Existing adaptive and state-aware conformal procedures mainly ask how calibration errors should be weighted, localized, or updated over time. By contrast, we study how strongly the correction itself should depend on the scale of the state variable.

2.3 Volatility Proxies, Regime Dependence, and the Gap Addressed Here

In financial risk applications, the relevant notion of state scale is often supplied by a volatility proxy. Because volatility is latent, practical risk measurement relies on proxies such as rolling volatility, GARCH-based forecasts, range-based estimators, and implied-volatility indices such as the VIX [Parkinson, 1980, Garman and Klass, 1980, Andersen and Bollerslev, 1998, Andersen et al., 2003, Poon and Granger, 2003, Whaley, 2009]. These quantities are informative but imperfect: some are backward-looking, some are model-dependent, and some embed risk premia or market frictions. In stressed markets, such imperfections become especially important, making volatility inputs themselves a source of model risk. Recent evidence also suggests that VIX dynamics and option-implied information continue to contain incremental predictive content for future volatility and tail-sensitive forecasting tasks [Bai and Cai, 2024, Michael et al., 2025].

This issue is closely connected to the broader literature on regime dependence, stressed-market dynamics, and state-dependent risk control [Hamilton, 1989, Ang and Bekaert, 2002, Glasserman et al., 2015, Adrian and Brunnermeier, 2016, Acharya et al., 2017, Ardia et al.,

2018]. When recalibration is driven by an imperfect volatility proxy, regime dependence matters not only because market conditions change, but also because proxy misspecification can become most consequential precisely in stressed states. This makes the relevant question not merely whether recalibration should respond to the environment, but how strongly the correction should scale with the proxy itself. These considerations motivate introducing a proxy-reliance parameter ρ , which measures how strongly the recalibration correction inherits the scale of an imperfect volatility signal. Larger values of ρ increase state responsiveness but also increase vulnerability to stressed-state proxy underreaction, whereas smaller values trade some responsiveness for robustness.

3 Data

3.1 Sample and Assets

Our empirical analysis uses daily data for six widely traded ETFs—SPY, QQQ, IWM, EEM, GLD, and TLT—covering broad U.S. equities, technology, small-cap equities, emerging-market equities, gold, and Treasuries. The raw panel sample runs from February 2, 2015 to December 29, 2025. ETF price and volume data are collected from the Twelve Data API at the 1-day frequency, and each ETF series is merged by trading date with the CBOE Volatility Index (VIX) for state measurement and stress classification. The six-asset panel provides the main cross-asset evidence across equity, rates, commodity, and emerging-market exposures, while SPY is retained as an illustrative single-asset benchmark within the same aligned sample.

For each ETF, the forecasting target is the one-day-ahead log return. Let $P_{i,t}$ denote the daily closing price of asset i on date t . We define

$$r_{i,t} = \log \left(\frac{P_{i,t}}{P_{i,t-1}} \right), \quad Y_{i,t} = r_{i,t+1}.$$

Thus, at time t , the forecasting problem is to estimate the lower α -quantile of $Y_{i,t}$, with $\alpha = 0.05$ in the baseline specification. Before constructing the modeling panel, observations are sorted by asset, date, and volume, duplicate (i, t) entries are removed by retaining the final record for

each asset-date pair, and the modeling sample is then formed by dropping rows with missing values in the target and required volatility-related predictors.

After feature construction and removal of observations with missing lagged inputs, the balanced panel retains 1,730 rolling one-step test forecasts per asset. All backtests are conducted in a strictly chronological out-of-sample manner and are analyzed both asset by asset and in pooled summaries.

3.2 Variables and Features

The predictor set combines recent return information, historical and range-based volatility measures, implied-volatility information, drawdown, and trading activity. Table 1 summarizes the main variables used in the baseline forecasting models and in the construction of state variables.

Table 1: Summary of forecasting variables and state features

Category	Variables	Role
Returns	$r_{i,t}, r_{i,t-1}, r_{i,t-2}, r_{i,t-3}, r_{i,t-5}$	Recent price dynamics and short-run persistence
Historical volatility	20-day rolling volatility; lagged volatility features	Time-varying risk information
EWMA volatility	EWMA volatility (span 20)	Smoothed volatility scale
Range-based proxies	Parkinson and Garman–Klass estimators	Intraday range-based risk information
Implied volatility	VIX-implied daily volatility; daily VIX percentage change	Forward-looking stress information
Drawdown	60-day rolling drawdown	Adverse market-state indicator
Trading activity	Log volume; rolling volume z -score	Activity and liquidity-related state information

Two variables play a central role in the market-state construction. First, the VIX level is converted into an approximate daily implied-volatility proxy. Let VIX_t denote the observed VIX level on date t . Then

$$v_t^{\text{VIX}} = \frac{VIX_t}{100\sqrt{252}}. \quad (1)$$

This transformation treats the VIX as a forward-looking volatility gauge rather than as ground truth, which is consistent with both classic interpretations of the index and the broader volatility-

forecasting literature [Poon and Granger, 2003, Whaley, 2009, Bai and Cai, 2024]. Second, the rolling 60-day drawdown is defined as

$$DD_{i,t}^{(60)} = \frac{P_{i,t}}{\max_{0 \leq j \leq 59} P_{i,t-j}} - 1. \quad (2)$$

In addition, we include a trading-activity feature based on volume. Let $\text{Volume}_{i,t}$ denote the trading volume of asset i on date t , and define

$$L_{i,t}^{\text{vol}} = \log(\text{Volume}_{i,t}), \quad (3)$$

which is standardized using a rolling 20-day mean and standard deviation.

These variables are not intended to form an exhaustive alpha model. Rather, they provide a compact and interpretable state representation for one-sided tail-risk forecasting and recalibration.

3.3 Volatility Proxy and Stress-State Definition

A central object in the paper is a positive volatility proxy v_t used to scale the recalibration adjustment. We construct a composite proxy from three components: 20-day rolling volatility, a GARCH-style volatility proxy, and the daily volatility transformation of the VIX. In implementation, the GARCH-style component is obtained from expanding-window conditional volatility estimates; detailed estimation and fallback rules are reported in Appendix C. To preserve comparability across components while keeping the final proxy in units comparable to rolling volatility, we first normalize each component by its in-sample median on the current training window and then re-anchor the average to the rolling-volatility component. Let $C = \{c_1, c_2, c_3\}$ denote the three components, and let $\mathcal{T}_{\text{train}}$ denote the current training-window index set. Define

$$m_j = \max\left(\text{median}\{c_{j,s} : s \in \mathcal{T}_{\text{train}}\}, 10^{-8}\right), \quad j = 1, 2, 3. \quad (4)$$

Let S denote the set of dates within the current rolling window on which the proxy is evaluated.

Then, for $t \in S$,

$$v_t = \left(\frac{1}{3} \sum_{j=1}^3 \frac{c_{j,t}}{m_j} \right) m_1. \quad (5)$$

Thus, the composite proxy is expressed in units comparable to the rolling-volatility component.

A small floor is imposed to ensure positivity:

$$v_t \leftarrow \max(v_t, 10^{-8}). \quad (6)$$

Market-state labels are generated without look-ahead bias. In each rolling training window, the distribution of v_t^{VIX} is used to define a three-bin regime partition:

- **low-stress regime:** v_t^{VIX} below the training median;
- **mid-stress regime:** v_t^{VIX} between the training median and the training 80th percentile;
- **high-stress regime:** v_t^{VIX} above the training 80th percentile.

For subgroup evaluation, we also define a stricter stress flag. Let $q_{0.90}^{(train)}(v^{\text{VIX}})$ denote the 90th percentile of the training-window VIX-based daily volatility proxy, and let $q_{0.30}^{(train)}(DD_i^{(60)})$ denote the 30th percentile of the training-window 60-day drawdown for asset i . Then

$$\mathbf{1}\{\text{stress}_t = 1\} = \mathbf{1}\left\{v_t^{\text{VIX}} \geq q_{0.90}^{(train)}(v^{\text{VIX}})\right\} \cdot \mathbf{1}\left\{DD_{i,t}^{(60)} \leq q_{0.30}^{(train)}(DD_i^{(60)})\right\}. \quad (7)$$

This rolling construction avoids look-ahead bias and ensures that stress is defined relative to the prevailing market environment rather than to the full sample.

3.4 Out-of-Sample Design

All results are produced under a strictly chronological rolling design. For each forecast origin, the available data are divided into a training window of 504 observations, a calibration-selection window of 252 observations, a final calibration window of 126 observations, and a one-step test point. Thus, all baseline forecasts, state thresholds, and recalibration quantities are formed using

only information available at the forecast date. The selection logic is described in Section 4, while additional implementation details are reported in Appendix C.

This design yields 1,730 one-step test forecasts per asset in the balanced panel and ensures that the reported results reflect genuine out-of-sample performance under time-varying market conditions.

4 Methodology

4.1 Baseline Forecasts and Proxy-Reliance-Controlled Recalibration

For clarity, we present the method for a generic asset; in the empirical analysis, the same rolling procedure is applied separately to each ETF in the panel. For notational simplicity, we suppress the asset index i in this section and write $Y_t = r_{t+1}$ for the next-period return realized after forecast origin t . Let $\widehat{q}_{\alpha,t}$ denote a baseline forecast of the lower α -quantile of Y_t , where $\alpha = 0.05$. Throughout the paper, VaR is expressed in return space, so more negative values correspond to more conservative left-tail forecasts. Our goal is to construct a one-sided left-tail VaR forecast

$$\widehat{\text{VaR}}_{\alpha,t} = \widehat{q}_{\alpha,t}^{adj}, \quad (8)$$

such that the exceedance probability

$$\mathbb{P}\left(Y_t \leq \widehat{\text{VaR}}_{\alpha,t}\right) \quad (9)$$

is close to α , both overall and in stressed market states.

Table 2 summarizes the baseline VaR forecasters considered in the empirical analysis. These baselines range from simple nonparametric rules to more structured parametric models, allowing us to assess whether the proposed recalibration layer adds value across different forecasting families. In the standalone SPY stronger-benchmark comparison, we also include AS-CAViaR as an auxiliary conditional-quantile benchmark. In the main-text pooled tables, we report GARCH- t as the representative parametric volatility family, while additional GJR-GARCH- t evidence is reported in Appendix B.

Table 2: Baseline VaR forecasters

Baseline	Definition
Historical simulation (HS)	Empirical α -quantile of training-window returns
Filtered historical simulation (FHS)	Empirical α -quantile of standardized training-window returns, rescaled by current EWMA volatility
Quantile regression (QR)	Linear quantile regression fitted on the full feature vector
GARCH-proxy quantile (GPQ)	Empirical standardized quantile based on a GARCH-style volatility proxy
GARCH- t	Parametric GARCH model with Student- t innovations
GJR-GARCH- t	Asymmetric GARCH model with Student- t innovations

Against this background, our methodological question is not how to replace the baseline forecaster, but how strongly the recalibration adjustment should depend on the volatility proxy that scales it.

The key tuning parameter is $\rho \in [0, 1]$, which controls how strongly the recalibration adjustment depends on the volatility proxy. Given a baseline VaR forecast $\widehat{q}_{\alpha,s}$ and a positive volatility proxy v_s , define the signed lower-tail residual at calibration date s by

$$u_s^{(\rho)} = \frac{Y_s - \widehat{q}_{\alpha,s}}{v_s^\rho}. \quad (10)$$

For the calibration index set \mathcal{I}_t associated with the current forecast origin t , define

$$c_{\rho,t} = Q_\alpha^{\text{lower}} \left(\left\{ u_s^{(\rho)} : s \in \mathcal{I}_t \right\} \right), \quad (11)$$

where Q_α^{lower} denotes the lower empirical α -quantile. The resulting one-step recalibrated forecast is

$$\widehat{q}_{\alpha,t}^{\text{adj}} = \widehat{q}_{\alpha,t} + c_{\rho,t} v_t^\rho. \quad (12)$$

This formulation nests two limiting cases. When $\rho = 0$, the recalibration behaves like an approximately constant shift. When $\rho = 1$, the correction fully inherits the scale of the proxy. Intermediate values interpolate continuously between these extremes. Thus, ρ measures how strongly the recalibration correction depends on proxy scale.

4.2 Formal Properties of Proxy Reliance

To formalize the role of ρ , define the signed adjustment

$$A_\rho(v; c) = c v^\rho, \quad (13)$$

where $c < 0$ is the lower-tail calibration constant and $v > 0$ is the proxy level. The following results are mechanism-based structural properties under stylized local assumptions, rather than finite-sample guarantees for the full rolling procedure. The first two results characterize clean-proxy scaling, while the third identifies stressed-state fragility under stress-specific proxy underreaction.

Proposition 4.1 (Elasticity and invariance under uniform proxy rescaling). *Fix $\rho \in [0, 1]$. For any $\eta > 0$,*

$$A_\rho(\eta v; c) = \eta^\rho A_\rho(v; c). \quad (14)$$

Hence the sensitivity of the adjustment magnitude to proportional changes in proxy scale is governed exactly by ρ . Moreover, if the proxy is uniformly rescaled by the same positive multiplicative factor at all calibration points and at the forecast point, while the baseline forecast is held fixed, then the resulting one-step recalibrated VaR forecast is unchanged.

Proposition 4.2 (Cross-state contrast induced by ρ). *Fix $c \neq 0$ and let $v_H > v_L > 0$ denote two proxy levels corresponding to a higher- and a lower-risk state. Then*

$$\frac{|A_\rho(v_H; c)|}{|A_\rho(v_L; c)|} = \left(\frac{v_H}{v_L}\right)^\rho. \quad (15)$$

Consequently, this contrast ratio is increasing in ρ , equals 1 at $\rho = 0$, and equals v_H/v_L at $\rho = 1$.

Propositions 4.1–4.2 show that ρ governs both the sensitivity of the adjustment to proxy scale and the contrast of the adjustment across market states. These results suggest focusing on heterogeneous, state-dependent distortion rather than uniform multiplicative rescaling.

Proposition 4.3 (Stress-state exceedance distortion under proxy underreaction). *Fix a forecast date t such that $\text{stress}_t = 1$, and an exponent $\rho \in [0, 1]$. Let*

$$q_{\rho,t}^* = \widehat{q}_{\alpha,t} + c_{\rho,t} v_t^\rho \quad (16)$$

denote the clean-proxy recalibrated forecast, where $c_{\rho,t} < 0$ is the clean-proxy recalibration constant associated with forecast origin t , and $v_t > 0$. Define

$$F_t(y) := \mathbb{P}(Y_t \leq y \mid \mathcal{F}_t), \quad (17)$$

where \mathcal{F}_t denotes the information set available at the forecast date t . Assume that under the clean proxy this forecast is conditionally exact at level α , namely

$$F_t(q_{\rho,t}^*) = \alpha. \quad (18)$$

Now suppose that the proxy underreacts multiplicatively at the forecast point,

$$\widetilde{v}_t = \kappa v_t, \quad \kappa \in (0, 1), \quad (19)$$

and define the misspecified forecast

$$\widetilde{q}_{\rho,t} = \widehat{q}_{\alpha,t} + c_{\rho,t} \widetilde{v}_t^\rho = \widehat{q}_{\alpha,t} + c_{\rho,t} \kappa^\rho v_t^\rho. \quad (20)$$

Then the conditional exceedance distortion

$$\Delta_t(\rho) := \mathbb{P}(Y_t \leq \widetilde{q}_{\rho,t} \mid \mathcal{F}_t) - \alpha \quad (21)$$

satisfies

$$\Delta_t(\rho) = F_t(\widetilde{q}_{\rho,t}) - F_t(q_{\rho,t}^*) \geq 0. \quad (22)$$

If, moreover, $\rho > 0$ and F_t is continuous on $[q_{\rho,t}^, \widetilde{q}_{\rho,t}]$ and differentiable on $(q_{\rho,t}^*, \widetilde{q}_{\rho,t})$,*

with derivative $f_t(y) := F'_t(y)$, then there exists some

$$\xi_{\rho,t} \in (q_{\rho,t}^*, \tilde{q}_{\rho,t}) \quad (23)$$

such that

$$\Delta_t(\rho) = f_t(\xi_{\rho,t}) |c_{\rho,t}| v_t^\rho (1 - \kappa^\rho). \quad (24)$$

For $\rho = 0$, one has $\tilde{q}_{\rho,t} = q_{\rho,t}^*$ and hence $\Delta_t(0) = 0$.

Consequently, for $\rho > 0$, if there exist constants

$$0 < \underline{f}_t \leq \bar{f}_t < \infty$$

such that

$$\underline{f}_t \leq f_t(y) \leq \bar{f}_t \quad \text{for all } y \in [q_{\rho,t}^*, \tilde{q}_{\rho,t}],$$

then

$$\underline{f}_t |c_{\rho,t}| v_t^\rho (1 - \kappa^\rho) \leq \Delta_t(\rho) \leq \bar{f}_t |c_{\rho,t}| v_t^\rho (1 - \kappa^\rho). \quad (25)$$

The same bounds hold trivially at $\rho = 0$, since $\Delta_t(0) = 0$.

Corollary 4.4 (Ordering under matched clean-proxy stress adjustment). *Under the assumptions of Proposition 4.3, suppose in addition that the clean-proxy signed adjustment magnitude is matched across ρ , i.e. there exists $a_t > 0$ such that*

$$|c_{\rho,t}| v_t^\rho = a_t \quad \text{for all } \rho \in [0, 1]. \quad (26)$$

Then, for $\rho > 0$,

$$\Delta_t(\rho) = f_t(\xi_{\rho,t}) a_t (1 - \kappa^\rho), \quad (27)$$

while $\Delta_t(0) = 0$.

If, moreover, there exist constants $0 < \underline{f}_t \leq \bar{f}_t < \infty$ such that

$$\underline{f}_t \leq f_t(y) \leq \bar{f}_t \quad \text{for all } y \in [q_{\rho,t}^*, \tilde{q}_{\rho,t}] \text{ and all } \rho \in (0, 1], \quad (28)$$

then for $\rho > 0$,

$$\underline{f}_t a_t (1 - \kappa^\rho) \leq \Delta_t(\rho) \leq \bar{f}_t a_t (1 - \kappa^\rho). \quad (29)$$

The same bounds hold trivially at $\rho = 0$.

Since $\kappa \in (0, 1)$, the map $\rho \mapsto 1 - \kappa^\rho$ is increasing on $[0, 1]$. Hence the exceedance distortion is nondecreasing in ρ up to the density factor. In particular, if the map $\rho \mapsto f_t(\xi_{\rho,t})$ is nondecreasing and strictly positive on $(0, 1]$, then $\Delta_t(\rho)$ is increasing in ρ on $(0, 1]$.

Taking conditional expectation over stressed forecast dates yields

$$\bar{\Delta}(\rho) := \mathbb{E}[\Delta_t(\rho) \mid \text{stress}_t = 1]. \quad (30)$$

Assuming the relevant quantities are integrable, the pointwise bounds above imply corresponding ρ -dependent conditional-expectation bounds for $\bar{\Delta}(\rho)$. Nondecreasing dependence on ρ follows under the additional condition that the map $\rho \mapsto f_t(\xi_{\rho,t})$ is constant or nondecreasing on $(0, 1]$; stronger monotonicity follows under the stricter positivity condition stated in Corollary 4.4. Proofs, together with a supplementary screening result, are collected in Appendix A.

4.3 Proxy-Reliance Selection and Regime-Aware Extension

Empirically, we use a nested rolling design. For each forecast origin t , candidate proxy-reliance rules are first selected on an intermediate selection block, and the final recalibration constant is then re-estimated on a separate calibration block before one-step evaluation. The exact window lengths and search grids are reported in Appendix C.

We consider two scalar selectors. Let \mathcal{R} denote the candidate set of proxy-reliance values, and let \mathcal{S}_t denote the intermediate selection block associated with forecast origin t . The *global average selector* chooses the proxy-reliance value that minimizes average capital on the selection block,

$$\hat{\rho}_t^{\text{global,avg}} = \arg \min_{\rho \in \mathcal{R}} \frac{1}{|\mathcal{S}_t|} \sum_{s \in \mathcal{S}_t} \max\left(-\hat{q}_{\alpha,s}^{\text{adj}}(\rho), 0\right), \quad (31)$$

where $\hat{q}_{\alpha,s}^{\text{adj}}(\rho)$ denotes the candidate-specific recalibrated forecast constructed on the selection block under proxy-reliance value ρ . This selector is intentionally capital-oriented and does not

impose additional stress-specific feasibility screening.

The *global stress-aware selector* instead prioritizes adverse-state tail control: candidates are screened using stress-sensitive and overall exceedance criteria, and among admissible candidates the selector trades off stress-period pinball loss and capital usage. Additional implementation details, including search grids, feasibility thresholds, and fallback rules, are reported in Appendix C.

After a scalar proxy-reliance value $\widehat{\rho}_t$ is selected at forecast origin t , the final recalibration constant is re-estimated on a separate calibration index set \mathcal{I}_t , yielding the one-step forecast

$$\widehat{q}_{\alpha,t}^{adj} = \widehat{q}_{\alpha,t} + c_{\widehat{\rho}_t,t} v_t^{\widehat{\rho}_t}, \quad (32)$$

where

$$c_{\widehat{\rho}_t,t} = Q_{\alpha}^{lower} \left(\left\{ \frac{Y_s - \widehat{q}_{\alpha,s}}{v_s^{\widehat{\rho}_t}} : s \in \mathcal{I}_t \right\} \right). \quad (33)$$

We also consider a regime-dependent extension. Let

$$g_t \in \{\text{low, mid, high}\} \quad (34)$$

denote the rolling regime label defined from the training-window VIX distribution, and let

$$\boldsymbol{\rho} = (\rho_{low}, \rho_{mid}, \rho_{high}) \quad (35)$$

denote a regime-specific proxy-reliance rule. For a given candidate tuple $\boldsymbol{\rho}$, define the regime-adjusted residual on the calibration sample by

$$u_s^{(\boldsymbol{\rho})} = \frac{Y_s - \widehat{q}_{\alpha,s}}{v_s^{\rho_{g_s}}}, \quad s \in \mathcal{I}_t, \quad (36)$$

and the corresponding recalibration constant by

$$c_{\boldsymbol{\rho},t} = Q_{\alpha}^{lower} \left(\left\{ u_s^{(\boldsymbol{\rho})} : s \in \mathcal{I}_t \right\} \right). \quad (37)$$

The associated one-step recalibrated forecast is

$$\widehat{q}_{\alpha,t}^{adj}(\boldsymbol{\rho}) = \widehat{q}_{\alpha,t} + c_{\rho,t} v_t^{\rho_{gt}}. \quad (38)$$

To preserve interpretability and reduce overfitting, we restrict attention to monotone tuples satisfying

$$\rho_{low} \geq \rho_{mid} \geq \rho_{high}. \quad (39)$$

This restriction reflects the hypothesis that proxy reliance should weaken in more stressed states. Let $\widehat{\boldsymbol{\rho}}_t$ denote the selected monotone tuple at forecast origin t ; the final regime-dependent forecast is then $\widehat{q}_{\alpha,t}^{adj}(\widehat{\boldsymbol{\rho}}_t)$.

4.4 Empirical Implementation and Evaluation

We study two proxy scenarios. Under the *clean proxy*, the composite volatility proxy is used as constructed. Under the *underreacting stress proxy*, the proxy is shrunk only in stressed states according to

$$v_t^{mis} = \begin{cases} \kappa v_t, & \text{if } \text{stress}_t = 1, \\ v_t, & \text{otherwise,} \end{cases} \quad \kappa \in (0, 1), \quad (40)$$

so that the proxy underreacts precisely where stressed-state tail control matters most. The reported implementation uses $\kappa = 0.4$; further implementation details are given in Appendix C.

Each method is evaluated in a one-step rolling backtest. For each forecast date, we record the realized return Y_t , the recalibrated forecast $\widehat{q}_{\alpha,t}^{adj}$, and the exceedance indicator

$$I_t = \mathbf{1}\{Y_t \leq \widehat{q}_{\alpha,t}^{adj}\}. \quad (41)$$

We report the unconditional exceedance frequency

$$\widehat{p} = \frac{1}{T} \sum_{t=1}^T I_t, \quad (42)$$

the strict-stress exceedance frequency

$$\widehat{p}_{strict} = \frac{\sum_{t=1}^T I_t \mathbf{1}\{\text{stress}_t^{strict} = 1\}}{\sum_{t=1}^T \mathbf{1}\{\text{stress}_t^{strict} = 1\}}, \quad (43)$$

where stress_t^{strict} denotes the rolling strict-stress flag defined in Section 3. In the empirical analysis, stress_t denotes the broader rolling stress indicator used in proxy misspecification and stress-aware selection, whereas stress_t^{strict} is used only for final stressed-state reporting. We also report the average capital

$$\frac{1}{T} \sum_{t=1}^T \max\left(-\widehat{q}_{\alpha,t}^{adj}, 0\right). \quad (44)$$

We also report quantile tick loss and standard VaR backtests, including the Kupiec unconditional coverage test, the Christoffersen conditional coverage test, and the Engle–Manganelli dynamic quantile (DQ) test.

5 Results

We organise the empirical results around the cross-asset panel and use SPY only as an illustrative benchmark. The six-ETF panel provides the main evidence across heterogeneous assets and baseline forecasters, while the aligned SPY slice visualises the same mechanisms in a familiar single-market setting. Each method is evaluated over 1,730 rolling one-step test dates per asset, for a pooled total of 10,380 out-of-sample forecasts.

5.1 Cross-asset panel evidence

We begin with pooled panel comparisons across the six ETFs. Table 3 shows that proxy-reliance-controlled recalibration does not deliver uniform improvements across pooled overall metrics. As shown below, its empirical gains are more concentrated in stressed-state tail performance.

Table 3 reports the pooled overall results. FHS and GPQ already perform strongly under the clean proxy. By contrast, historical simulation undercovers the tail, with exceedance 0.0598, and quantile regression is more distorted, with exceedance 0.0925. Recalibration moves both much closer to the nominal 5% target, although at a capital cost. For GARCH- t , the raw model is

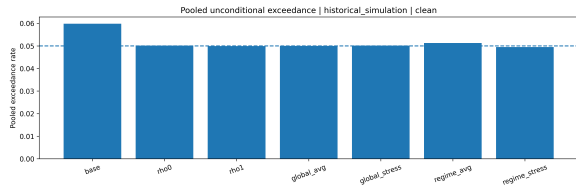
overly conservative, and recalibration releases much of this conservatism while lowering average capital toward 0.023, although conditional-coverage and DQ diagnostics remain weak. This indicates that recalibration repairs unconditional and stress-sensitive coverage more reliably than it removes all dynamic dependence misspecification in tail violations. Additional GJR-GARCH- t results lead to the same qualitative conclusion; see Appendix B.

Table 3: Pooled overall out-of-sample results across the six-asset panel under the clean proxy specification. Exceedance denotes pooled unconditional breach frequency. Avg cap. denotes average capital proxy. UC, CC, and DQ indicate whether the pooled Kupiec, Christoffersen, and Engle–Manganelli dynamic quantile (DQ) tests are passed at the 5% level.

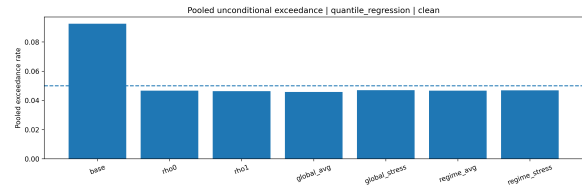
Baseline	Method	Exceed.	Avg cap.	Tick loss	UC	CC	DQ
FHS	Base	0.0497	0.0205	0.001415	Y	Y	N
FHS	$\rho = 0$	0.0487	0.0216	0.001461	Y	Y	N
FHS	$\rho = 1$	0.0468	0.0223	0.001464	Y	Y	N
FHS	Global-stress	0.0481	0.0219	0.001461	Y	Y	N
FHS	Regime-stress	0.0476	0.0225	0.001499	Y	Y	N
GPQ	Base	0.0516	0.0201	0.001384	Y	Y	N
GPQ	$\rho = 0$	0.0487	0.0211	0.001411	Y	Y	N
GPQ	$\rho = 1$	0.0472	0.0215	0.001415	Y	Y	N
GPQ	Global-stress	0.0485	0.0213	0.001414	Y	Y	N
GPQ	Regime-stress	0.0477	0.0217	0.001432	Y	Y	N
HS	Base	0.0598	0.0188	0.001598	N	N	N
HS	$\rho = 0$	0.0501	0.0211	0.001525	Y	N	N
HS	$\rho = 1$	0.0499	0.0208	0.001469	Y	N	N
HS	Global-stress	0.0501	0.0211	0.001489	Y	N	N
HS	Regime-stress	0.0495	0.0218	0.001558	Y	N	N
QR	Base	0.0925	0.0180	0.001791	N	N	N
QR	$\rho = 0$	0.0466	0.0229	0.001566	Y	N	N
QR	$\rho = 1$	0.0463	0.0228	0.001526	Y	N	N
QR	Global-stress	0.0469	0.0227	0.001535	Y	N	N
QR	Regime-stress	0.0468	0.0246	0.001620	Y	N	N
GARCH- t	Base	0.0472	0.0323	0.002137	Y	N	N
GARCH- t	$\rho = 0$	0.0434	0.0228	0.001553	N	N	N
GARCH- t	$\rho = 1$	0.0472	0.0236	0.001650	Y	N	N
GARCH- t	Global-stress	0.0453	0.0232	0.001563	N	N	N
GARCH- t	Regime-stress	0.0447	0.0245	0.001665	N	N	N

Figure 1 visualises the pooled overall exceedance comparisons. The main message is that recalibration repairs weak baselines, but does not uniformly dominate the strongest raw proxy-aware benchmarks in tick loss or capital usage.

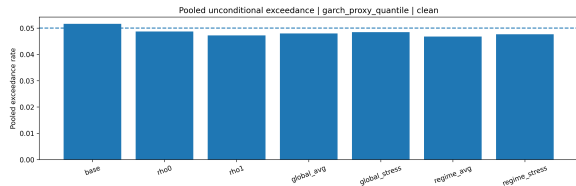
The panel results also show substantial cross-asset heterogeneity. Figure 2 shows that the value of recalibration depends on both the baseline family and the asset. The largest raw distortions arise for historical simulation and quantile regression, whereas FHS and GPQ are already more stable across assets. The clearest repair cases are QQQ and SPY. For example, the raw GPQ baseline for QQQ has overall exceedance 0.0566 and strict-stress exceedance 0.0718; using $\rho = 0$ lowers these to 0.0497 and 0.0462, respectively, at higher capital. For SPY, the raw



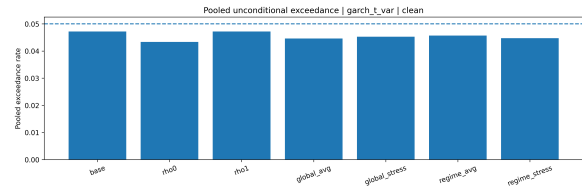
(a) Historical simulation



(b) Quantile regression

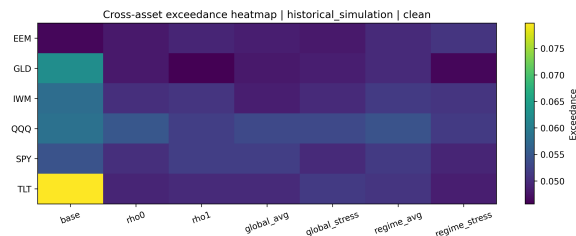


(c) GARCH-proxy quantile

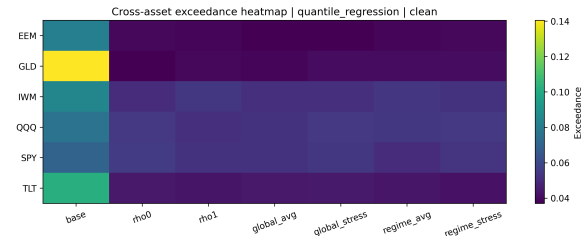


(d) GARCH- t VaR

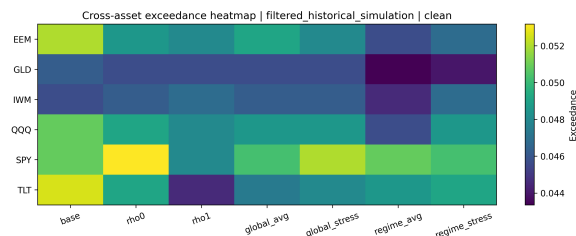
Figure 1: Pooled overall exceedance across the six-asset panel under the clean proxy specification. The dashed horizontal line marks the nominal 5% target.



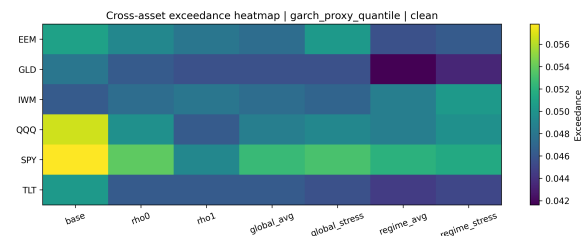
(a) Historical simulation



(b) Quantile regression



(c) Filtered historical simulation



(d) GARCH-proxy quantile

Figure 2: Cross-asset exceedance heatmaps under the clean proxy specification.

GPQ baseline moves from 0.0578 overall and 0.0894 under strict stress to 0.0514 overall and 0.0447 under the regime-stress rule. By contrast, IWM, GLD, and TLT already have raw GPQ performance close to target, leaving less room for improvement. Figure 3 summarizes these exceedance–capital trade-offs.

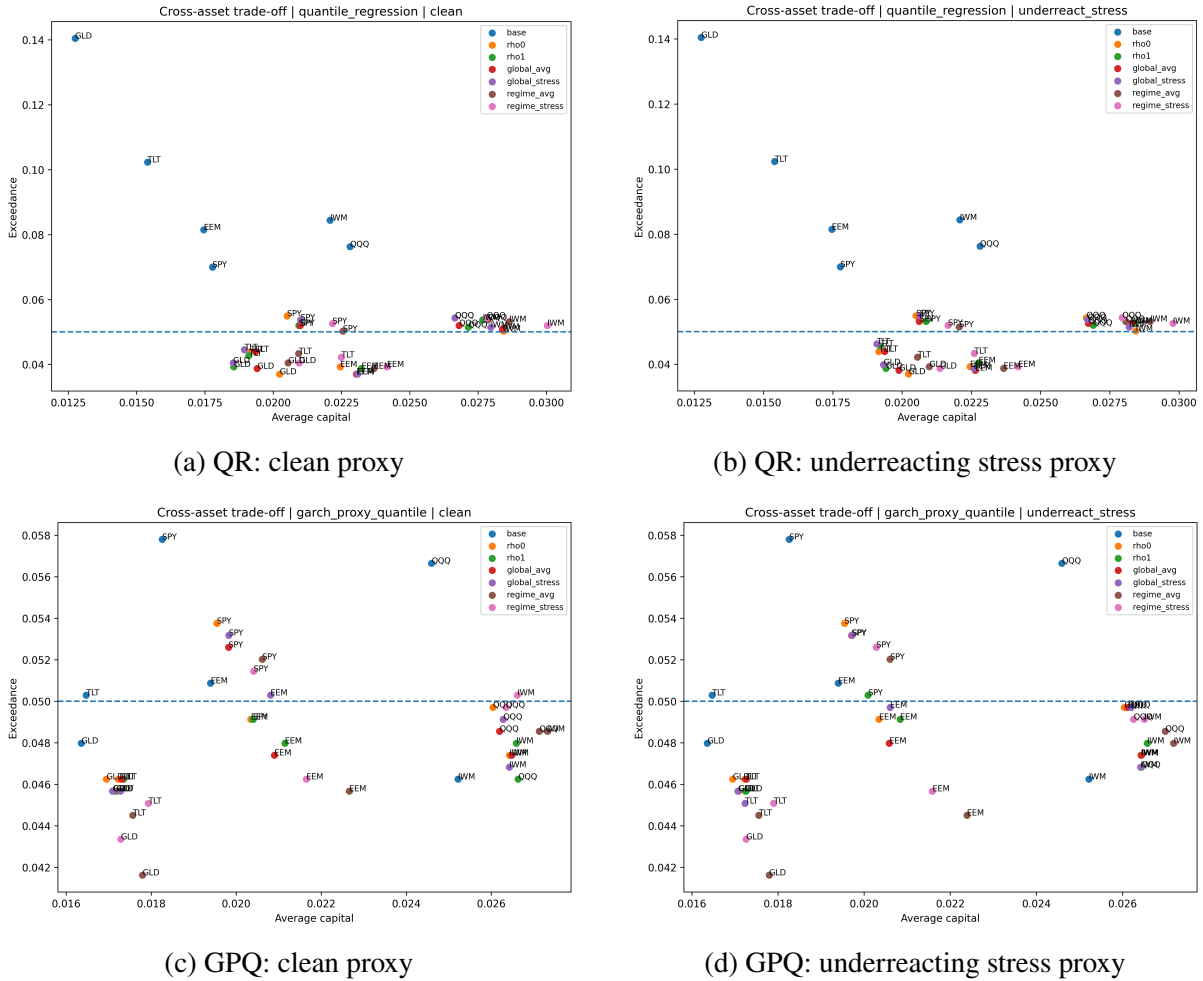


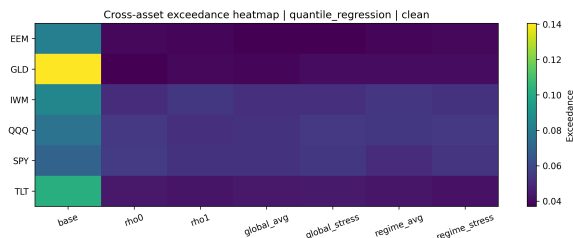
Figure 3: Cross-asset exceedance–capital trade-offs for two representative baseline families.

A second panel-level result concerns robustness under proxy underreaction. Table 4 shows that the main deterioration appears in stressed states rather than in pooled overall performance. This deterioration is concentrated in high- ρ rules. For example, for HS the stressed exceedance of $\rho = 1$ worsens from 0.0622 under the clean proxy to 0.0873 under proxy underreaction, and for QR it worsens from 0.0512 to 0.0693. By contrast, GPQ with $\rho = 0$ remains essentially unchanged at 0.0462, and the GPQ global-stress selector is likewise stable. This pattern is consistent with Proposition 4.3 and Corollary 4.4: stronger proxy dependence increases fragility when the proxy underreacts precisely in stressed states. Figure 4 shows the same robustness pattern across assets.

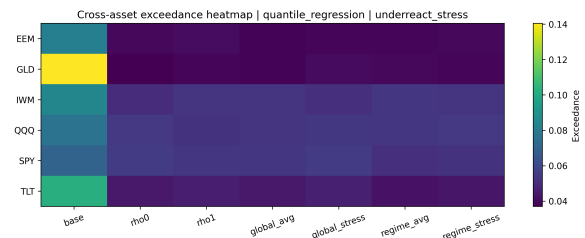
Taken together, the panel evidence suggests that proxy-reliance-controlled recalibration is best viewed as a model-agnostic repair mechanism whose empirical value is concentrated in stressed-state robustness under proxy imperfection rather than in uniform overall dominance.

Table 4: Pooled strict-stress robustness under clean and underreacting-stress proxy specifications. Stress exceed. denotes pooled strict-stress exceedance; stressed cap. denotes pooled strict-stress average capital.

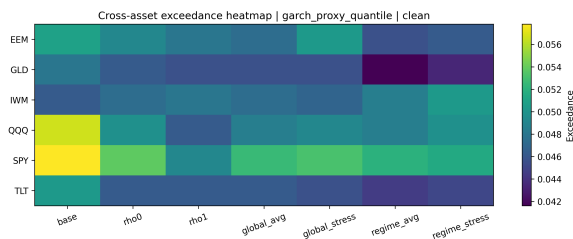
Baseline	Method	Clean stress exceed.	Underreact stress exceed.	Clean stressed cap.	Underreact stressed cap.
HS	Base	0.1717	0.1717	0.0141	0.0141
HS	$\rho = 0$	0.0783	0.0783	0.0294	0.0294
HS	$\rho = 1$	0.0622	0.0873	0.0304	0.0265
HS	Global-stress	0.0703	0.0894	0.0306	0.0271
QR	Base	0.2209	0.2209	0.0218	0.0218
QR	$\rho = 0$	0.0592	0.0592	0.0368	0.0368
QR	$\rho = 1$	0.0512	0.0693	0.0379	0.0327
QR	Global-stress	0.0552	0.0703	0.0368	0.0323
GPQ	Base	0.0612	0.0612	0.0325	0.0325
GPQ	$\rho = 0$	0.0462	0.0462	0.0363	0.0363
GPQ	$\rho = 1$	0.0402	0.0472	0.0398	0.0366
GPQ	Global-stress	0.0462	0.0462	0.0374	0.0363
GARCH- t	Base	0.1446	0.1446	0.0261	0.0261
GARCH- t	$\rho = 0$	0.0723	0.0723	0.0307	0.0307
GARCH- t	$\rho = 1$	0.0763	0.0813	0.0308	0.0308
GARCH- t	Global-stress	0.0683	0.0803	0.0311	0.0299



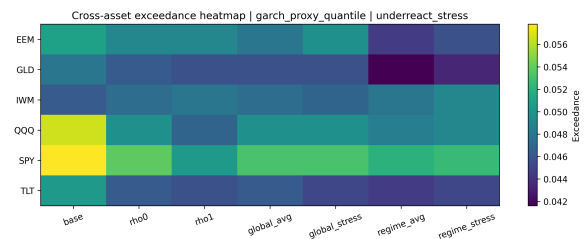
(a) QR: clean proxy



(b) QR: underreacting stress proxy



(c) GPQ: clean proxy



(d) GPQ: underreacting stress proxy

Figure 4: Cross-asset exceedance heatmaps under clean and underreacting-stress proxy specifications.

Its value is greatest when the raw baseline undercovers the left tail, especially in stressed states, whereas already strong proxy-aware baselines leave less room for improvement. The robustness experiments further support interpreting ρ as a trust parameter on the volatility proxy.

Table 5: Main SPY overall out-of-sample results under the clean proxy specification. Exceedance denotes the unconditional breach frequency. Avg cap. denotes the average capital proxy. UC, CC, and DQ indicate whether the Kupiec, Christoffersen, and Engle–Manganelli dynamic quantile (DQ) tests are passed at the 5% level.

Baseline	Method	Exceed.	Avg cap.	Tick loss	UC	CC	DQ
HS	Base	0.054	0.018	0.001689	Y	N	N
HS	$\rho = 0$	0.050	0.021	0.001571	Y	Y	N
HS	$\rho = 1$	0.052	0.020	0.001472	Y	Y	N
HS	Global-stress	0.050	0.021	0.001507	Y	Y	N
HS	Regime-stress	0.049	0.021	0.001524	Y	Y	N
FHS	Base	0.051	0.019	0.001387	Y	Y	N
FHS	$\rho = 0$	0.053	0.021	0.001469	Y	Y	N
FHS	$\rho = 1$	0.048	0.021	0.001445	Y	Y	N
FHS	Global-stress	0.052	0.021	0.001451	Y	Y	N
FHS	Regime-stress	0.050	0.022	0.001478	Y	Y	N
QR	Base	0.070	0.018	0.001429	N	N	N
QR	$\rho = 0$	0.055	0.021	0.001470	Y	Y	N
QR	$\rho = 1$	0.052	0.021	0.001433	Y	Y	N
QR	Global-stress	0.054	0.021	0.001463	Y	Y	N
QR	Regime-stress	0.053	0.022	0.001521	Y	Y	N
GPQ	Base	0.058	0.018	0.001339	Y	Y	Y
GPQ	$\rho = 0$	0.054	0.020	0.001357	Y	Y	N
GPQ	$\rho = 1$	0.049	0.020	0.001364	Y	Y	N
GPQ	Global-stress	0.053	0.020	0.001368	Y	Y	N
GPQ	Regime-stress	0.051	0.020	0.001362	Y	Y	Y
GARCH- t	Base	0.035	0.033	0.002274	N	N	N
GARCH- t	$\rho = 0$	0.046	0.023	0.001606	Y	Y	N
GARCH- t	$\rho = 1$	0.049	0.023	0.001649	Y	N	N
GARCH- t	Global-stress	0.046	0.023	0.001587	Y	N	N
GARCH- t	Regime-stress	0.045	0.024	0.001642	Y	N	N

5.2 SPY as an illustrative benchmark

The aligned SPY slice is included only to illustrate the panel mechanisms in a familiar single-market benchmark. Table 5 delivers the same qualitative ranking. QR remains the clearest repair case, with recalibration moving exceedance materially closer to target. FHS and GPQ are already relatively well calibrated on the aligned SPY sample, so recalibration mainly reshapes the coverage–capital and stress-control trade-off rather than generating large unconditional gains. For GARCH- t , recalibration releases excess conservatism while bringing exceedance closer to target. Additional aligned-SPY results for GJR-GARCH- t are reported in Appendix B.

5.3 Detailed SPY case study: comparison with stronger raw tail baselines

To assess whether the proposed recalibration layer adds value beyond weaker benchmark families, we also compare it against AS-CAViaR in an auxiliary standalone-SPY benchmark run. This auxiliary standalone-SPY run is based on a separate SPY-only rolling sample with 1,822

one-step forecasts, whereas the aligned SPY slice in the balanced six-asset panel contains 1,730 forecasts; the two exercises are therefore not numerically identical. AS-CAViaR is included because it is specifically designed for conditional quantile dynamics and, in this auxiliary benchmark exercise, delivers one of the strongest raw overall performances among the benchmark models. We also report GPQ as the strongest proxy-aware comparator.

Table 6 shows the role of the proposed method against stronger raw tail benchmarks. For both AS-CAViaR and GPQ, the raw baselines already perform strongly in unconditional terms, with acceptable exceedance, low tick loss, and successful UC/CC/DQ diagnostics. In this benchmark exercise, differences across recalibrated variants appear mainly in stress-period performance rather than in overall ranking.

Table 6: Auxiliary standalone-SPY comparison against stronger raw tail baselines under the clean proxy specification. These results are reported on a standalone SPY sample and are therefore not numerically identical to the aligned SPY slice in Tables 5 and 7. Stress exceed. denotes exceedance on the strict-stress subset. Backtests report UC/CC/DQ pass indicators at the 5% level.

Baseline	Method	Exceed.	Stress exceed.	Avg cap.	Tick loss	Backtests
AS-CAViaR	Base	5.87%	7.32%	0.0177	0.001324	Y/Y/Y
AS-CAViaR	$\rho = 1$	5.49%	5.37%	0.0195	0.001365	Y/Y/Y
AS-CAViaR	Global-stress	5.43%	5.85%	0.0192	0.001360	Y/Y/Y
AS-CAViaR	Regime-stress	5.54%	5.37%	0.0201	0.001404	Y/Y/N
GPQ	Base	5.98%	8.78%	0.0183	0.001350	Y/Y/Y
GPQ	$\rho = 1$	4.88%	5.37%	0.0202	0.001374	Y/Y/N
GPQ	Global-stress	5.54%	5.85%	0.0198	0.001372	Y/Y/N
GPQ	Regime-stress	5.38%	4.88%	0.0201	0.001382	Y/Y/N

5.3.1 Stress-period illustration

The stressed SPY results in Table 7 are consistent with the panel-level message that stressed performance is the main margin of interest. The historical-simulation baseline deteriorates sharply under strict stress, with stressed exceedance 0.240, and recalibration reduces this substantially, although not fully to target. GPQ again provides the strongest stressed case among the representative models: the regime-stress rule lowers strict-stress exceedance from 0.089 to 0.045. QR also moves close to target under stress after recalibration. These SPY results therefore reinforce the panel conclusion that the method is most useful as a robustness layer for stressed-tail control.

Table 7: SPY strict stress-period results under the clean proxy specification. Stress exceed. denotes the breach frequency conditional on the rolling strict stress flag. Stress gap is measured relative to the nominal 5% target. Avg cap. is the full-sample average capital proxy shown for reference.

Baseline	Method	Stress exceed.	Stress gap	Avg cap.
HS	Base	0.240	0.190	0.018
HS	$\rho = 0$	0.095	0.045	0.021
HS	$\rho = 1$	0.067	0.017	0.020
HS	Global-stress	0.078	0.028	0.021
HS	Regime-stress	0.078	0.028	0.021
FHS	Base	0.078	0.028	0.019
FHS	$\rho = 0$	0.073	0.023	0.021
FHS	$\rho = 1$	0.061	0.011	0.021
FHS	Global-stress	0.067	0.017	0.021
FHS	Regime-stress	0.061	0.011	0.022
QR	Base	0.089	0.039	0.018
QR	$\rho = 0$	0.056	0.006	0.021
QR	$\rho = 1$	0.045	-0.005	0.021
QR	Global-stress	0.050	0.000	0.021
QR	Regime-stress	0.050	0.000	0.022
GPQ	Base	0.089	0.039	0.018
GPQ	$\rho = 0$	0.061	0.011	0.020
GPQ	$\rho = 1$	0.050	0.000	0.020
GPQ	Global-stress	0.061	0.011	0.020
GPQ	Regime-stress	0.045	-0.005	0.020
GARCH- t	Base	0.184	0.134	0.033
GARCH- t	$\rho = 0$	0.095	0.045	0.023
GARCH- t	$\rho = 1$	0.078	0.028	0.023
GARCH- t	Global-stress	0.078	0.028	0.023
GARCH- t	Regime-stress	0.078	0.028	0.024

The SPY robustness and regime-selection diagnostics are also aligned with the panel evidence. Under stress-specific proxy underreaction, deterioration is concentrated in higher- ρ variants, while GPQ remains comparatively stable. Let $\bar{\rho}_{low}$, $\bar{\rho}_{mid}$, and $\bar{\rho}_{high}$ denote the sample averages of the selected regime-specific proxy-reliance levels over the rolling forecast origins. These average regime-dependent selections satisfy

$$\bar{\rho}_{low} > \bar{\rho}_{mid} > \bar{\rho}_{high},$$

indicating weaker proxy dependence in more stressed states. This pattern is structurally meaningful, although it does not translate into uniform predictive dominance over simpler scalar rules. Overall, the SPY evidence supports the same conclusion as the panel: proxy-reliance-controlled recalibration is most useful where stressed tail undercoverage remains after the baseline forecast is formed, and ρ governs how strongly the recalibration correction depends on the volatility proxy.

6 Discussion

The results identify *proxy reliance* as a distinct design choice in one-sided VaR recalibration. Rather than treating proxy scaling as an implicit feature of state-aware adjustment, the framework makes that dependence explicit and allows its stressed-state implications to be studied directly. Volatility signals are informative but not ground truth: the same proxy that improves state sensitivity in normal times can become a source of stressed-state fragility when it underreacts precisely where downside protection matters most.

The empirical and theoretical results point to the same takeaway: the decisive margin is stressed-state fragility rather than average performance. Several baselines that appear acceptable in pooled coverage deteriorate materially on the rolling strict-stress subset, and the gains from recalibration are more consistent on that margin than in aggregate unconditional metrics. The proxy-misspecification experiments sharpen the interpretation of ρ : when the proxy underreacts in adverse states, deterioration appears mainly in stressed exceedance and is more pronounced for higher- ρ rules. Empirically, ρ behaves like a trust parameter on the volatility proxy: larger values deliver greater state responsiveness, while smaller values provide more protection against proxy error.

The regime-dependent extension is most useful as a structural diagnostic rather than as a uniformly superior forecasting rule. The selected tuples are often economically sensible, with weaker proxy reliance in more stressed states, although they do not deliver uniform gains over simpler scalar rules. The same pattern appears in the auxiliary AS-CAViaR comparison: when the raw tail model is already strong, proxy-reliance-controlled recalibration is best viewed as a complementary robustness device. Its role is to strengthen stressed-state control rather than to substitute for the baseline forecasting model.

The proposed method is a recalibration framework rather than a full dynamic tail model. It often restores unconditional coverage and can improve conditional coverage, although dynamic quantile diagnostics remain challenging in many specifications. These DQ rejections indicate that residual serial structure in tail violations can persist after one-sided recalibration, because dynamic misspecification and proxy reliance are related but distinct problems. The paper therefore contributes a focused answer to a narrower but important question: how strongly

a one-sided recalibration adjustment should depend on an imperfect volatility proxy when stress-period protection is the priority. On this dimension, both the theoretical results and the stress-period evidence are economically informative.

Several limitations remain. The empirical study is restricted to six liquid daily U.S.-traded ETFs and a common VIX-linked state proxy; the analysis is confined to one-day-ahead left-tail VaR at the 5% level; and the regime-aware specification uses a deliberately coarse three-bin partition with a monotone restriction on $(\rho_{low}, \rho_{mid}, \rho_{high})$. In addition, the stress-aware selector uses a looser stressed subset during selection than during final reporting, reflecting stressed-sample scarcity. Natural extensions include richer state variables and alternative proxies, smoother state-dependent proxy-reliance maps, tighter integration with stronger dynamic tail models, and applications to other one-sided risk functionals such as expected shortfall.

7 Conclusion

This paper studies one-sided VaR recalibration through the lens of *proxy reliance*, which we formalize by a parameter $\rho \in [0, 1]$ that governs how strongly the left-tail adjustment scales with a volatility proxy.

The main finding is that proxy reliance matters most when stressed-state undercoverage interacts with proxy imperfection. The theoretical results show that larger ρ increases responsiveness to proxy scale but also raises fragility under proxy underreaction, while the empirical results show that lower or intermediate proxy reliance can outperform fully proxy-scaled recalibration in such settings. The regime-dependent extension provides structural insight but limited incremental predictive benefit over simpler global rules.

Overall, the paper shows that, when volatility proxies are informative yet imperfect, proxy reliance should itself be treated as a separate and explicit design choice in one-sided VaR recalibration.

A Proofs and supplementary theoretical results

This appendix collects the proofs of the main theoretical results and records two supplementary propositions that are omitted from the main text for expositional focus.

A.1 Supplementary propositions

Proposition A.1 (Heterogeneous proxy distortion and directional forecast shift). *Fix an exponent $\rho \in [0, 1]$ and a forecast date t . Let*

$$u_s^{(\rho)} = \frac{Y_s - \widehat{q}_{\alpha,s}}{v_s^\rho}, \quad s \in \mathcal{I},$$

denote the clean-proxy calibration residuals on a calibration sample \mathcal{I} , and let

$$c_\rho = Q_\alpha^{\text{lower}}\left(\{u_s^{(\rho)} : s \in \mathcal{I}\}\right)$$

be the corresponding clean-proxy lower-tail recalibration constant. Suppose the proxy is distorted multiplicatively according to

$$\widetilde{v}_s = d_s v_s, \quad s \in \mathcal{I}, \quad \text{and} \quad \widetilde{v}_t = d_t v_t,$$

where all distortion factors are strictly positive. Define the distorted calibration constant

$$\widetilde{c}_\rho = Q_\alpha^{\text{lower}}\left(\{d_s^{-\rho} u_s^{(\rho)} : s \in \mathcal{I}\}\right),$$

and the distorted forecast

$$\widetilde{q}_{\rho,t} = \widehat{q}_{\alpha,t} + \widetilde{c}_\rho \widetilde{v}_t^\rho.$$

Assume that the clean-proxy recalibration constant satisfies $c_\rho < 0$.

If

$$d_t \leq d_s \quad \text{for all } s \in \mathcal{I},$$

then

$$\tilde{q}_{\rho,t} \geq \widehat{q}_{\alpha,t} + c_{\rho} v_t^{\rho}.$$

If instead

$$d_t \geq d_s \quad \text{for all } s \in \mathcal{I},$$

then

$$\tilde{q}_{\rho,t} \leq \widehat{q}_{\alpha,t} + c_{\rho} v_t^{\rho}.$$

Consequently, if the clean-proxy forecast is conditionally exact at level α , where

$$F_t(y) := \mathbb{P}(Y_t \leq y \mid \mathcal{F}_{t-1}, \text{stress}_t = 1),$$

and

$$F_t(\widehat{q}_{\alpha,t} + c_{\rho} v_t^{\rho}) = \alpha,$$

then forecast-point underreaction that is at least as severe as calibration-sample underreaction yields nonnegative conditional exceedance distortion, while the reverse ordering yields nonpositive conditional exceedance distortion.

Proposition A.2 (Selection implication under stress screening). *Suppose that under stress-specific proxy underreaction the average stressed-state exceedance distortion*

$$\bar{\Delta}(\rho) := \mathbb{E}[\Delta_t(\rho) \mid \text{stress}_t = 1]$$

is continuous and nondecreasing on $[0, 1]$. Assume moreover that under the matched clean-proxy adjustment condition there exists a nonnegative process a_t such that the distorted stressed-state forecast can be written as

$$\tilde{q}_{\rho,t} = \widehat{q}_{\alpha,t} - a_t \kappa^{\rho}, \quad \kappa \in (0, 1),$$

for stressed forecast dates. Define the stressed-state average capital proxy

$$\bar{K}(\rho) := \mathbb{E}[\max(-\tilde{q}_{\rho,t}, 0) \mid \text{stress}_t = 1].$$

Then $\bar{K}(\rho)$ is nonincreasing in ρ .

For a stress tolerance $\tau \geq 0$, consider the screened selector

$$\hat{\rho}(\tau) \in \arg \min_{\rho \in \mathcal{R}} \bar{K}(\rho) \quad \text{subject to} \quad \bar{\Delta}(\rho) \leq \tau,$$

where $\mathcal{R} \subset [0, 1]$ is the candidate grid.

Then the feasible set is of the form

$$\mathcal{F}(\tau) = \mathcal{R} \cap [0, \rho_{\max}(\tau)]$$

for some $\rho_{\max}(\tau) \in [0, 1]$ (possibly with empty feasible set), and any minimizer can be taken to be the largest feasible candidate. In particular, if

$$0 \leq \tau_1 \leq \tau_2,$$

then

$$\hat{\rho}(\tau_1) \leq \hat{\rho}(\tau_2).$$

Hence tightening the stressed-state exceedance tolerance weakly lowers the selected proxy reliance.

A.2 Proofs

Proof of Proposition 4.1. For any $\eta > 0$,

$$A_\rho(\eta v; c) = c(\eta v)^\rho = \eta^\rho c v^\rho = \eta^\rho A_\rho(v; c),$$

which proves the homogeneity statement. Taking logs yields

$$\log |A_\rho(\eta v; c)| = \log |c| + \rho \log \eta + \rho \log v,$$

so

$$\frac{\partial \log |A_\rho(\eta v; c)|}{\partial \log \eta} = \rho.$$

Now suppose $\tilde{v}_t = \eta v_t$ for all calibration and test points. The signed residual becomes

$$\tilde{u}_t^{(\rho)} = \frac{Y_t - \widehat{q}_{\alpha,t}}{(\eta v_t)^\rho} = \eta^{-\rho} u_t^{(\rho)}.$$

Since $\eta^{-\rho} > 0$ and the lower empirical conformal quantile is positively homogeneous,

$$\tilde{c}_\rho = Q_\alpha^{\text{lower}}(\{\tilde{u}_t^{(\rho)}\}) = Q_\alpha^{\text{lower}}(\{\eta^{-\rho} u_t^{(\rho)}\}) = \eta^{-\rho} Q_\alpha^{\text{lower}}(\{u_t^{(\rho)}\}) = \eta^{-\rho} c_\rho.$$

Therefore the final signed adjustment at the forecast point satisfies

$$\tilde{c}_\rho (\tilde{v}_t)^\rho = \eta^{-\rho} c_\rho (\eta v_t)^\rho = c_\rho v_t^\rho,$$

and hence the recalibrated forecast is unchanged. \square

Proof of Proposition 4.2. Since $A_\rho(v; c) = cv^\rho$,

$$\frac{|A_\rho(v_H; c)|}{|A_\rho(v_L; c)|} = \frac{|c|v_H^\rho}{|c|v_L^\rho} = \left(\frac{v_H}{v_L}\right)^\rho.$$

Because $v_H/v_L > 1$, this ratio is increasing in ρ . At $\rho = 0$ it equals 1, and at $\rho = 1$ it equals v_H/v_L . \square

Proof of Proposition A.1. Write

$$a_s := \left(\frac{d_t}{d_s}\right)^\rho, \quad s \in \mathcal{I}.$$

Using positive homogeneity of the lower empirical quantile, we have

$$\tilde{c}_\rho = Q_\alpha^{lower} \left(\{d_s^{-\rho} u_s^{(\rho)} : s \in \mathcal{I}\} \right),$$

and hence

$$\tilde{q}_{\rho,t} = \hat{q}_{\alpha,t} + d_t^\rho v_t^\rho Q_\alpha^{lower} \left(\{d_s^{-\rho} u_s^{(\rho)} : s \in \mathcal{I}\} \right) = \hat{q}_{\alpha,t} + v_t^\rho Q_\alpha^{lower} \left(\{a_s u_s^{(\rho)} : s \in \mathcal{I}\} \right).$$

Define

$$x_s := a_s u_s^{(\rho)}, \quad s \in \mathcal{I}.$$

First suppose that $d_t \leq d_s$ for all $s \in \mathcal{I}$. Then $a_s \leq 1$ for all $s \in \mathcal{I}$. We claim that for every $z < 0$,

$$\{x_s \leq z\} \subseteq \{u_s^{(\rho)} \leq z\}.$$

Indeed, if $x_s \leq z < 0$, then necessarily $u_s^{(\rho)} \leq 0$, because $a_s > 0$. Since $a_s \leq 1$ and $u_s^{(\rho)} \leq 0$, the inequality

$$a_s u_s^{(\rho)} \leq z$$

implies

$$u_s^{(\rho)} \leq \frac{z}{a_s} \leq z.$$

Therefore

$$\{x_s \leq z\} \subseteq \{u_s^{(\rho)} \leq z\}.$$

It follows that the empirical distribution function of $\{x_s\}$ is pointwise no larger than that of $\{u_s^{(\rho)}\}$ on the negative half-line. Since $c_\rho < 0$ is the lower α -quantile of the clean residuals, we obtain

$$Q_\alpha^{lower}(\{x_s : s \in \mathcal{I}\}) \geq Q_\alpha^{lower}(\{u_s^{(\rho)} : s \in \mathcal{I}\}) = c_\rho.$$

Hence

$$\tilde{q}_{\rho,t} = \hat{q}_{\alpha,t} + v_t^\rho Q_\alpha^{lower}(\{x_s : s \in \mathcal{I}\}) \geq \hat{q}_{\alpha,t} + c_\rho v_t^\rho.$$

Now suppose instead that $d_t \geq d_s$ for all $s \in \mathcal{I}$. Then $a_s \geq 1$ for all $s \in \mathcal{I}$. For every $z < 0$,

if $u_s^{(\rho)} \leq z$, then necessarily $u_s^{(\rho)} \leq 0$, and so

$$x_s = a_s u_s^{(\rho)} \leq u_s^{(\rho)} \leq z.$$

Thus

$$\{u_s^{(\rho)} \leq z\} \subseteq \{x_s \leq z\}.$$

Therefore the empirical distribution function of $\{x_s\}$ is pointwise no smaller than that of $\{u_s^{(\rho)}\}$ on the negative half-line, which implies

$$Q_\alpha^{lower}(\{x_s : s \in \mathcal{I}\}) \leq c_\rho.$$

Consequently,

$$\tilde{q}_{\rho,t} \leq \widehat{q}_{\alpha,t} + c_\rho v_t^\rho.$$

For the final claim, if

$$F_t(\widehat{q}_{\alpha,t} + c_\rho v_t^\rho) = \alpha,$$

then monotonicity of F_t implies that an upward shift in the forecast threshold yields nonnegative exceedance distortion, whereas a downward shift yields nonpositive exceedance distortion. \square

Proof of Proposition 4.3. If $\rho > 0$, then $\kappa^\rho < 1$. Since $c_{\rho,t} < 0$, we have

$$\tilde{q}_{\rho,t} = \widehat{q}_{\alpha,t} + c_{\rho,t} \kappa^\rho v_t^\rho > \widehat{q}_{\alpha,t} + c_{\rho,t} v_t^\rho = q_{\rho,t}^*.$$

If $\rho = 0$, then $\kappa^\rho = 1$, so

$$\tilde{q}_{\rho,t} = q_{\rho,t}^*.$$

Therefore, for all $\rho \in [0, 1]$,

$$F_t(\tilde{q}_{\rho,t}) - F_t(q_{\rho,t}^*) \geq 0.$$

Using the conditional exactness assumption $F_t(q_{\rho,t}^*) = \alpha$, it follows that

$$\Delta_t(\rho) = F_t(\tilde{q}_{\rho,t}) - F_t(q_{\rho,t}^*) \geq 0.$$

If moreover F_t is differentiable on $(q_{\rho,t}^*, \tilde{q}_{\rho,t})$, then for $\rho > 0$ the mean-value theorem yields some

$$\xi_{\rho,t} \in (q_{\rho,t}^*, \tilde{q}_{\rho,t})$$

such that

$$F_t(\tilde{q}_{\rho,t}) - F_t(q_{\rho,t}^*) = f_t(\xi_{\rho,t})(\tilde{q}_{\rho,t} - q_{\rho,t}^*).$$

Since

$$\tilde{q}_{\rho,t} - q_{\rho,t}^* = c_{\rho,t} \kappa^\rho v_t^\rho - c_{\rho,t} v_t^\rho = |c_{\rho,t}| v_t^\rho (1 - \kappa^\rho),$$

this proves (24) for $\rho > 0$. For $\rho = 0$, both sides of (24) equal 0. The bounds in (25) then follow immediately from

$$\underline{f}_t \leq f_t(\xi_{\rho,t}) \leq \bar{f}_t.$$

□

Proof of Corollary 4.4. Substituting the matched-adjustment condition

$$|c_\rho| v_t^\rho = a_t$$

into Proposition 4.3 gives

$$\Delta_t(\rho) = f_t(\xi_{\rho,t}) a_t (1 - \kappa^\rho),$$

and likewise

$$\underline{f}_t a_t (1 - \kappa^\rho) \leq \Delta_t(\rho) \leq \bar{f}_t a_t (1 - \kappa^\rho).$$

Since $\kappa \in (0, 1)$,

$$\frac{d}{d\rho} (1 - \kappa^\rho) = -\kappa^\rho \log \kappa > 0,$$

so the factor $1 - \kappa^\rho$ is increasing in ρ . Therefore $\Delta_t(\rho)$ is increasing in ρ up to the density factor. In particular, if $f_t(\xi_{\rho,t})$ is constant in ρ , or more generally nondecreasing, then $\Delta_t(\rho)$ is increasing in ρ . □

Proof of Proposition A.2. Since $\kappa \in (0, 1)$, the map $\rho \mapsto \kappa^\rho$ is decreasing on $[0, 1]$. Therefore

for each stressed forecast date t ,

$$\tilde{q}_{\rho,t} = \hat{q}_{\alpha,t} - a_t \kappa^\rho$$

is nondecreasing in ρ , because $a_t \geq 0$. Since the function

$$x \mapsto \max(-x, 0)$$

is nonincreasing in x , it follows that

$$\max(-\tilde{q}_{\rho,t}, 0)$$

is nonincreasing in ρ for each stressed date t . Taking conditional expectation gives that $\bar{K}(\rho)$ is nonincreasing in ρ .

Next, since $\bar{\Delta}(\rho)$ is continuous and nondecreasing on $[0, 1]$, the sublevel set

$$\{\rho \in [0, 1] : \bar{\Delta}(\rho) \leq \tau\}$$

is an interval of the form $[0, \rho_{\max}(\tau)]$ or is empty. Intersecting with the finite candidate grid \mathcal{R} yields

$$\mathcal{F}(\tau) = \mathcal{R} \cap [0, \rho_{\max}(\tau)].$$

Because $\bar{K}(\rho)$ is nonincreasing in ρ , minimizing $\bar{K}(\rho)$ over the feasible set is equivalent to choosing the largest feasible candidate. Therefore any minimizer can be taken as

$$\hat{\rho}(\tau) = \max \mathcal{F}(\tau),$$

whenever the feasible set is nonempty.

Finally, if $0 \leq \tau_1 \leq \tau_2$, then

$$\{\rho : \bar{\Delta}(\rho) \leq \tau_1\} \subseteq \{\rho : \bar{\Delta}(\rho) \leq \tau_2\},$$

so

$$\mathcal{F}(\tau_1) \subseteq \mathcal{F}(\tau_2).$$

Hence

$$\max \mathcal{F}(\tau_1) \leq \max \mathcal{F}(\tau_2),$$

which implies

$$\widehat{\rho}(\tau_1) \leq \widehat{\rho}(\tau_2).$$

This proves that tighter stressed-state tolerance weakly lowers the selected proxy reliance. \square

B Additional GJR-GARCH- t results

Table 8: Additional SPY clean-proxy results for the GJR-GARCH- t baseline. Exceed. and Avg cap. are computed on the full aligned SPY test sample. Stress exceed. and Stress cap. are computed on the rolling strict-stress subset. Tick loss denotes full-sample quantile tick loss.

Method	Exceed.	Stress exceed.	Avg cap.	Stress cap.	Tick loss	UC	CC	DQ
Base	0.0503	0.2402	0.0197	0.0119	0.001700	Y	N	N
$\rho = 0$	0.0503	0.0950	0.0210	0.0335	0.001600	Y	Y	N
$\rho = 1$	0.0514	0.0838	0.0202	0.0335	0.001500	Y	N	N
Global-average	0.0491	0.0782	0.0208	0.0344	0.001500	Y	Y	N
Global-stress	0.0497	0.0894	0.0205	0.0340	0.001500	Y	Y	N
Regime-average	0.0549	0.0838	0.0215	0.0392	0.001600	Y	N	N
Regime-stress	0.0462	0.0726	0.0216	0.0381	0.001500	Y	Y	N

C Additional Implementation Details

C.1 Rolling design

All empirical results are produced in a strictly chronological rolling design. For each forecast origin, the sample is divided into a training window of 504 observations, a calibration-selection window of 252 observations, a final calibration window of 126 observations, and a one-step test point. The calibration-selection window is split into a ρ -fit block of 84 observations and a ρ -evaluation block of 168 observations.

At each forecast origin, the baseline VaR model is fitted on the training block only. Candidate proxy-reliance rules are compared on the calibration-selection block. After a rule has been selected, the recalibration constant is re-estimated on the final calibration block and applied to the one-step test forecast. All regime thresholds, stress flags, proxy normalizations, and recalibration quantities are recomputed within each rolling window using only information available at the forecast date.

C.2 Composite volatility proxy

The volatility proxy used in the recalibration layer combines 20-day rolling volatility, a GARCH-style volatility proxy, and the VIX-based daily volatility transformation. Let $C = \{c_1, c_2, c_3\}$ denote these components. Within each rolling training window, each component is normalized by its in-sample median,

$$m_j = \max(\text{median}(c_j), 10^{-8}), \quad j = 1, 2, 3,$$

and the proxy on subset S is defined by

$$v_t = \left(\frac{1}{3} \sum_{j=1}^3 \frac{c_{j,t}}{m_j} \right) m_1, \quad t \in S.$$

A small floor is imposed to ensure positivity,

$$v_t \leftarrow \max(v_t, 10^{-8}).$$

In implementation, the GARCH-style component is obtained from expanding-window one-step-ahead conditional volatility estimates whenever the `arch` package is available; otherwise, or when a local fit fails, the corresponding proxy value is replaced by the EWMA volatility estimate.

C.3 Baseline forecasters

Table 9 summarizes the baseline VaR forecasters used in the empirical analysis.

Table 9: Baseline VaR forecasters used in the implementation.

Baseline	Implementation summary
Historical simulation (HS)	Empirical α -quantile of training-window returns.
Filtered historical simulation (FHS)	Let σ_t^{EWMA} denote <code>ewma_vol_20</code> . We compute the empirical lower-tail quantile of $(Y_t - \bar{Y}) / \sigma_t^{\text{EWMA}}$ on the training block and rescale by the current EWMA volatility level.
Quantile regression (QR)	Linear quantile regression fitted on the full predictor vector after feature standardization, implemented as a <code>StandardScaler</code> followed by <code>QuantileRegressor</code> with quantile level α , L_1 -penalty parameter 10^{-4} , and <code>highs</code> solver. The predictor vector includes return lags, historical and EWMA volatility measures, the GARCH-style volatility proxy, Parkinson and Garman–Klass range proxies, VIX-based variables, drawdown, and rolling volume features.
GARCH-proxy (GPQ)	quantile Let σ_t^{GPQ} denote <code>garch_vol_proxy</code> . We compute the empirical lower-tail quantile of $(Y_t - \bar{Y}) / \sigma_t^{\text{GPQ}}$ on the training block and rescale by the current proxy level. When the GARCH-style proxy is unavailable at a given point, it is replaced by <code>ewma_vol_20</code> .
GARCH- t VaR	Parametric constant-mean GARCH(1,1) model with Student- t innovations, fitted on training returns and used to generate the implied lower-tail quantile path over the evaluation horizon.
GJR-GARCH- t VaR	Parametric constant-mean GJR-GARCH(1,1) model with Student- t innovations, fitted on training returns and used to generate the implied lower-tail quantile path over the evaluation horizon.

For the GARCH-style proxy used in GPQ and in the composite recalibration proxy, we compute expanding-window one-step-ahead conditional volatility estimates with a lookback length of 252 observations whenever the `arch` package is available. The proxy fit uses a constant-mean GARCH(1,1) specification with normal innovations. If the package is unavailable or a local fit fails, the corresponding proxy value is replaced by `ewma_vol_20`.

For the GARCH- t and GJR-GARCH- t baselines, the fitted model generates a multi-step path of conditional lower-tail quantiles over the relevant evaluation block. If a parametric volatility fit fails, the implementation falls back to historical simulation for that rolling window. In the auxiliary standalone SPY benchmark comparison, AS-CAViaR is also included as a stronger raw tail benchmark and is estimated by bounded multi-start optimization of the asymmetric CAViaR quantile-loss objective.

C.4 Proxy-reliance selection

For the scalar specification, candidate values are searched over

$$\mathcal{R} = \{0, 0.1, 0.2, \dots, 1.0\}.$$

For each $\rho \in \mathcal{R}$, the recalibration constant is estimated on the ρ -fit block and the resulting forecast is evaluated on the ρ -evaluation block.

Two scalar selectors are used. The *global average selector* chooses the candidate with the smallest average capital proxy on the evaluation block. The *global stress-aware selector* instead emphasizes adverse-state control using a looser stress subset. The initial selection-stage stress threshold is based on the 70th percentile of the rolling training-window VIX-based daily volatility measure and is relaxed, if necessary, until a minimum stressed count is reached. A candidate is treated as feasible if its stress-period exceedance and overall exceedance remain within prespecified tolerances; among feasible candidates, the selector trades off stress-period pinball loss and average capital, while infeasible cases are handled by a penalized objective.

For the regime-dependent specification, the rolling training-window VIX distribution defines low-, medium-, and high-stress regimes through the median and 80th percentile cutoffs. Candidate rules are searched over monotone tuples

$$(\rho_{low}, \rho_{mid}, \rho_{high}), \quad \rho_{low} \geq \rho_{mid} \geq \rho_{high},$$

with each component drawn from

$$\{0, 0.25, 0.50, 0.75, 1.0\}.$$

For each candidate tuple, a single recalibration constant is estimated after scaling residuals by the regime-specific exponent. The regime-average selector trades off average capital and a smoothness penalty, while the regime-stress selector replaces the scalar stress subset with the high-stress regime and applies an analogous feasibility-and-penalty logic.

C.5 Proxy misspecification and evaluation

Two proxy scenarios are studied. Under the *clean proxy*, the composite volatility proxy is used as constructed. Under the *underreacting stress proxy*, the proxy is shrunk on stress dates according to

$$v_t^{mis} = \kappa v_t, \quad \kappa = 0.4.$$

In the reported implementation, the stress dates used in this misspecification experiment are defined by the rolling strict-stress rule in the main text.

For each forecast date, the implementation records the realized return, the baseline VaR forecast, the recalibrated VaR forecast, the signed recalibration shift, the exceedance indicator, the selected proxy-reliance level, and the associated regime and stress labels. Reported performance metrics include unconditional exceedance, strict-stress exceedance, average capital, quantile tick loss, the Kupiec unconditional coverage test, the Christoffersen conditional coverage test, and a DQ-style dynamic quantile diagnostic.

Disclosure statement

The authors report no potential conflict of interest.

Funding

No external funding was received for this research.

Data availability statement

The data used in this study were obtained from public sources cited in the text, including the Twelve Data API (<https://api.twelvedata.com>) and publicly available VIX data. Processed data and replication materials are available to the editor and reviewers upon reasonable request during the review process.

Code availability

Code used to generate the empirical results is available to the editor and reviewers upon reasonable request during the review process. A public replication repository will be provided after the review process.

References

- Viral V. Acharya, Lasse H. Pedersen, Thomas Philippon, and Matthew Richardson. Measuring systemic risk. *Rev. Financ. Stud.*, 30(1):2–47, 2017. doi: 10.1093/rfs/hhw088.
- Tobias Adrian and Markus K. Brunnermeier. CoVaR. *Am. Econ. Rev.*, 106(7):1705–1741, 2016. doi: 10.1257/aer.20120555.
- Agnideep Aich, Ashit Baran Aich, and Dipak C. Jain. Temporal conformal prediction (TCP): A distribution-free statistical and machine learning framework for adaptive risk forecasting, 2025. URL <https://arxiv.org/abs/2507.05470>. arXiv preprint.
- Torben G. Andersen and Tim Bollerslev. Answering the skeptics: yes, standard volatility models do provide accurate forecasts. *Int. Econ. Rev.*, 39(4):885–905, 1998. doi: 10.2307/2527343.
- Torben G. Andersen, Tim Bollerslev, Francis X. Diebold, and Paul Labys. Modeling and forecasting realized volatility. *Econometrica*, 71(2):579–625, 2003. doi: 10.1111/1468-0262.00418.
- Andrew Ang and Geert Bekaert. International asset allocation with regime shifts. *Rev. Financ. Stud.*, 15(4):1137–1187, 2002. doi: 10.1093/rfs/15.4.1137.
- Anastasios N. Angelopoulos and Stephen Bates. Conformal prediction: A gentle introduction. *Found. Trends Mach. Learn.*, 16(4):494–591, 2023. doi: 10.1561/2200000101.
- David Ardía, Keven Bluteau, Kris Boudt, and Leopoldo Catania. Forecasting risk with markov-switching GARCH models: A large-scale performance study. *Int. J. Forecast.*, 34(4):733–747, 2018. doi: 10.1016/j.ijforecast.2018.05.004.
- Yunfei Bai and Charlie X. Cai. Predicting VIX with adaptive machine learning. *Quant. Finance*, 24(12):1857–1873, 2024. doi: 10.1080/14697688.2024.2439458.
- Giovanni Barone-Adesi, Kostas Giannopoulos, and Les Vosper. VaR without correlations for portfolios of derivative securities. *J. Futures Mark.*, 19(5):583–602, 1999. doi: 10.1002/(SICI)1096-9934(199908)19:5<583::AID-FUT5>3.0.CO;2-S.

- Basel Committee on Banking Supervision. Minimum capital requirements for market risk. Technical report, Bank for International Settlements, 2019. URL <https://www.bis.org/bcbs/publ/d457.htm>. Corrected version published 25 February 2019.
- Osbert Bastani, Varun Gupta, Christopher Jung, Georgy Noarov, Ramya Ramalingam, and Aaron Roth. Practical adversarial multivalid conformal prediction. In *Advances in Neural Information Processing Systems 35*, pages 29362–29373, 2022. URL https://proceedings.neurips.cc/paper_files/paper/2022/hash/bcdaaa1aec3ae2aa39542acefdec4e4b-Abstract-Conference.html.
- Tim Bollerslev. Generalized autoregressive conditional heteroskedasticity. *J. Econom.*, 31(3): 307–327, 1986. doi: 10.1016/0304-4076(86)90063-1.
- Victor Chernozhukov, Kaspar Wüthrich, and Yinchu Zhu. Exact and robust conformal inference methods for predictive machine learning with dependent data. In *Proceedings of the 31st Conference on Learning Theory*, volume 75 of *Proceedings of Machine Learning Research*, pages 732–749. PMLR, 2018. URL <https://proceedings.mlr.press/v75/chernozhukov18a.html>.
- Peter F. Christoffersen. Evaluating interval forecasts. *Int. Econ. Rev.*, 39(4):841–862, 1998. doi: 10.2307/2527341.
- Peter F. Christoffersen. *Elements of financial risk management*. Academic Press, Waltham, MA, 2nd edition, 2012.
- Robert F. Engle. Autoregressive conditional heteroscedasticity with estimates of the variance of united kingdom inflation. *Econometrica*, 50(4):987–1007, 1982. doi: 10.2307/1912773.
- Robert F. Engle and Simone Manganelli. CAViaR: Conditional autoregressive value at risk by regression quantiles. *J. Bus. Econ. Stat.*, 22(4):367–381, 2004. doi: 10.1198/073500104000000370.
- Dean Fantazzini. Adaptive conformal inference for computing market risk measures: An analysis with four thousand crypto-assets. *J. Risk Financial Manag.*, 17(6):248, 2024. doi: 10.3390/jrfm17060248.

- Mark B. Garman and Michael J. Klass. On the estimation of security price volatilities from historical data. *J. Bus.*, 53(1):67–78, 1980. doi: 10.1086/296072.
- Isaac Gibbs and Emmanuel J. Candès. Adaptive conformal inference under distribution shift. In *Advances in Neural Information Processing Systems 34*, pages 1660–1672, 2021. URL https://proceedings.neurips.cc/paper_files/paper/2021/hash/0d441de75945e5acbc865406fc9a2559-Abstract.html.
- Paul Glasserman, Chulmin Kang, and Wanmo Kang. Stress scenario selection by empirical likelihood. *Quant. Finance*, 15(1):25–41, 2015. doi: 10.1080/14697688.2014.926019.
- James D. Hamilton. A new approach to the economic analysis of nonstationary time series and the business cycle. *Econometrica*, 57(2):357–384, 1989. doi: 10.2307/1912559.
- John Hull and Alan White. Incorporating volatility updating into the historical simulation method for value-at-risk. *J. Risk*, 1(1):5–19, 1998. doi: 10.21314/JOR.1998.001.
- Masahiro Kato. Conformal predictive portfolio selection, 2024. URL <https://arxiv.org/abs/2410.16333>. arXiv preprint.
- Roger Koenker. *Quantile regression*, volume 38 of *Econometric Society Monographs*. Cambridge University Press, Cambridge, 2005. doi: 10.1017/CBO9780511754098.
- Paul H. Kupiec. Techniques for verifying the accuracy of risk measurement models. *J. Derivatives*, 3(2):73–84, 1995. doi: 10.3905/jod.1995.407942.
- Nikolas Michael, Mihai Cucuringu, and Sam Howison. Options-driven volatility forecasting. *Quant. Finance*, 25(3):443–470, 2025. doi: 10.1080/14697688.2025.2454623.
- Fernando Moreno-Pino and Stefan Zohren. DeepVol: volatility forecasting from high-frequency data with dilated causal convolutions. *Quant. Finance*, 24(8):1105–1127, 2024. doi: 10.1080/14697688.2024.2387222.
- Michael Parkinson. The extreme value method for estimating the variance of the rate of return. *J. Bus.*, 53(1):61–65, 1980. doi: 10.1086/296071.

- Ser-Huang Poon and Clive W. J. Granger. Forecasting volatility in financial markets: A review. *J. Econ. Lit.*, 41(2):478–539, 2003. doi: 10.1257/002205103765762743.
- Marc Schmitt. Taming tail risk in financial markets: conformal risk control for nonstationary portfolio VaR, 2026. URL <https://arxiv.org/abs/2602.03903>. arXiv preprint.
- Giuseppe Storti and Chao Wang. A semi-parametric dynamic conditional correlation framework for risk forecasting. *Quant. Finance*, 25(1):31–49, 2025. doi: 10.1080/14697688.2024.2446740.
- Vladimir Vovk, Alexander Gammerman, and Glenn Shafer. *Algorithmic learning in a random world*. Springer, New York, NY, 2005. doi: 10.1007/b106715.
- Du-Yi Wang, Guo Liang, Kun Zhang, and Qianwen Zhu. Reliable real-time value at risk estimation via quantile regression forest with conformal calibration, 2026. URL <https://arxiv.org/abs/2602.01912>. arXiv preprint.
- Robert E. Whaley. Understanding the VIX. *J. Portf. Manag.*, 35(3):98–105, 2009. doi: 10.3905/JPM.2009.35.3.098.
- Chen Xu, Hanyang Jiang, and Yao Xie. Conformal prediction for multi-dimensional time series by ellipsoidal sets. In *Proceedings of the 41st International Conference on Machine Learning*, volume 235 of *Proceedings of Machine Learning Research*, pages 55076–55099. PMLR, 2024. URL <https://proceedings.mlr.press/v235/xu24m.html>.
- Jingyan Zhang, Cong Ma, and Wim Schoutens. Forward-looking physical tail risk: a deep learning approach. *Quant. Finance*, 2026. doi: 10.1080/14697688.2026.2623897. Published online 25 February 2026.